

Experimental and Computational Evaluation of Tantalocene Hydrides for C–H Activation of Arenes

Steven M. Rehbein, Matthew J. Kania, and Sharon R. Neufeldt*

Cite This: *Organometallics* 2021, 40, 2666–2677

Read Online

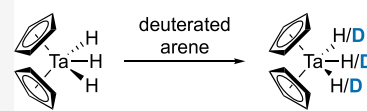
ACCESS |

Metrics & More

Article Recommendations

Supporting Information

ABSTRACT: Half a century ago, tantalocene hydrides (especially Cp_2TaH_3 , where $\text{Cp} = \eta^5\text{-C}_5\text{H}_5$) were reported to catalyze H/D exchange with arenes. However, there has been very little follow-up to the seminal reports, and numerous questions about this chemistry remain unanswered. In an effort to better evaluate the potential of tantalocene hydrides for processes involving C–H



- mechanism?
- conditions: Δ vs. $h\nu$?
- aromatic vs. benzylic C–H activation?
- ligand effects?

activation, we have conducted a series of experimental and computational studies on these complexes. Density functional theory (DFT) calculations support a mechanism for arene C–H activation involving oxidative addition at transient Ta^{III} , rather than a σ -bond metathesis mechanism at Ta^{V} . Comparisons were made between thermal and photochemical conditions for the reaction of Cp_2TaH_3 with benzene- d_6 , and H/D exchange was found to be moderately faster under thermal conditions. In a reaction with toluene, Cp_2TaH_3 activates the aromatic $\text{C}_{(\text{sp}^2)}\text{–H}$ bonds but not the benzylic bonds. DFT calculations suggest that benzylic C–H activation at Ta^{III} has a barrier similar to aromatic C–H activation, but that formation of a π -complex with Cp_2TaH directs preferential aromatic C–H activation. Analogous complexes containing the less labile permethylated ligand Cp^* ($\text{Cp}^* = \eta^5\text{-C}_5\text{Me}_5$) were also evaluated for their ability to catalyze H/D exchange with benzene- d_6 , but these complexes are less active than Cp_2TaH_3 . DFT calculations indicate that the methyl groups of Cp^* disfavor π -coordination of an arene to the Ta^{III} intermediate.

INTRODUCTION

Early transition metals are underexplored as molecular catalysts for organic transformations. Compared to their later counterparts, early metals often present more significant challenges with respect to air- and functional-group sensitivity.¹ Furthermore, low-valent early transition metals are highly reducing and electropositive. As a consequence, these metals tend to be most stable in high oxidation states, and redox cycling is more difficult compared to many late transition metals.² Because of these characteristics, development of early transition metal catalysis lags behind the success of late metals.³ Nevertheless, the same properties that make early metals challenging to work with also lend them unique potential as catalysts. Because they are so highly reducing, low-valent early transition metals often readily react with strong bonds such as C–H^4 or dinitrogen.⁵ Furthermore, early transition metals can participate in elementary reactions that are less common with late metals (e.g., σ -bond metathesis and α -elimination).⁶ As such, it is possible to imagine using early transition metals to develop novel catalytic processes that exploit unusual combinations of elementary steps.

The activation and functionalization of hydrocarbons is one area in which early transition metals show potential for unique reactivity. C–H activation is known to occur across $\text{M}=\text{X}$ and $\text{M}\equiv\text{X}$ multiple bonds ($\text{X} = \text{C}$ or N). Examples include 1,2-addition at titanium alkylidynes⁷ or at tantalum imides.⁸ Alternatively, C–H activation can take place by σ -bond metathesis^{6c} or by oxidative addition.⁹ Basset and Copéret reported that silica-supported single-site tantalum hydrides can

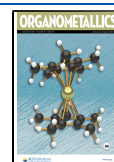
effect alkane coupling,¹⁰ metathesis,¹¹ and hydrogenolysis¹² through mechanisms involving C–H activation at Ta^{III} by oxidative addition^{13,14} or by σ -bond metathesis at Ta^{V} .^{10–12} Additionally, a number of reports have described activation of hydrocarbons by tantalum ions in the gas phase.¹⁵

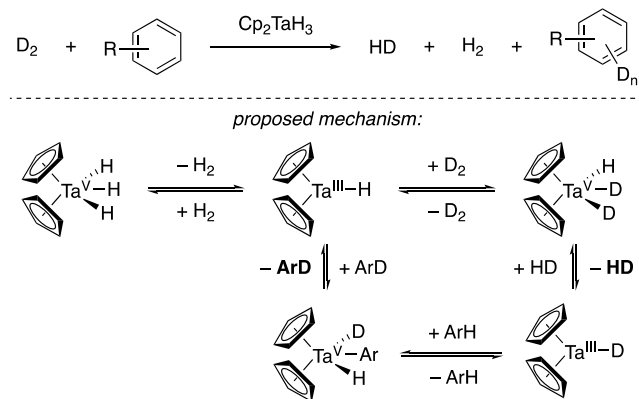
Inspired by this precedent, we have been interested in understanding how ligand environment and reaction conditions influence the reactivity of homogeneous tantalum hydrides with C–H bonds. The bent metallocene Cp_2TaH_3 ($\text{Cp} = \eta^5\text{-C}_5\text{H}_5$) was investigated in the 1970s and early 1980s for its ability to catalyze H/D exchange between arenes and D_2 (Scheme 1).¹⁶ This reaction was proposed to proceed through oxidative addition of C–H at transient $\text{Cp}_2\text{Ta}^{\text{III}}\text{H}$, suggesting that Cp ligands are sufficiently bulky and π -accepting to stabilize electron-rich Ta^{III} . Interestingly, Cp_2TaH_3 failed to catalyze benzylic H/D exchange using toluene or *para*-xylene, even though benzylic C–H bonds are weaker and more acidic than aromatic bonds.^{16d}

There has been almost no follow-up to the original publications using Cp_2TaH_3 for arene activation. As a result, the extent of this class of compound's potential for use in

Received: May 23, 2021

Published: July 14, 2021

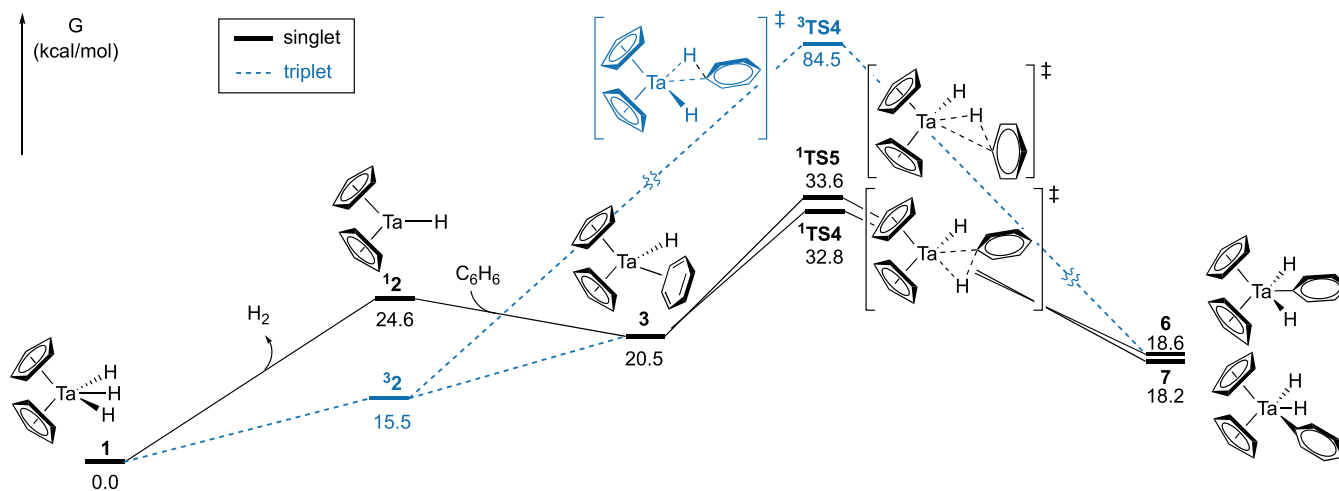


Scheme 1. H/D Exchange Catalyzed by Cp_2TaH_3 ¹⁶

catalytic C–H activation is nebulous. In particular, several questions about the chemistry shown in Scheme 1 remain unanswered. These questions include

1. What is the mechanism of C–H activation by Cp_2TaH_3 ? (Hydrocarbon activation at analogous silica-supported tantalum hydrides has been proposed to occur through both oxidative addition^{13,14} and σ -bond metathesis mechanisms.^{10–12})
2. How do thermal^{16a–d} versus photochemical^{16e} conditions compare for arene C–H activation? (Both conditions have been reported in the literature.)
3. Why are benzylic $\text{C}_{(\text{sp}^3)}\text{–H}$ bonds unreactive toward activation by Cp_2TaH_3 ?^{16d}
4. How does the reactivity of tantalocene hydrides bearing less labile permethylated ligands ($\text{CpCp}^*\text{TaH}_3$ and $\text{Cp}_2^*\text{TaH}_3$, where $\text{Cp}^* = \eta^5\text{-C}_5\text{Me}_5$) compare to that of Cp_2TaH_3 ?

Herein, we describe a combination of computational and experimental studies that provide insights into these fundamental questions. Developing a better understanding of the chemistry between tantalocene hydrides and arenes may facilitate future exploration of these complexes' reactivity toward more challenging aliphatic hydrocarbons.

Scheme 2. Calculated Pathways for the Reaction of Cp_2TaH_3 with Benzene via an Oxidative Addition Mechanism for C–H Activation

RESULTS AND DISCUSSION

In the early 1970s, Parshall and co-workers reported that both Cp_2TaH_3 and $\text{Cp}^{\text{Me}}_2\text{TaH}_3$ ($\text{Cp}^{\text{Me}} = \eta^5\text{-MeC}_5\text{H}_4$) catalyze H/D exchange between arenes and D_2 (or between deuterated arenes and H_2) upon heating to $\sim 100^\circ\text{C}$.^{16a–d} This claim was based on isotope scrambling in the products observed by mass spectrometry, including HD and partially deuterated arenes (Scheme 1). The mechanism of C–H activation was proposed to proceed through a $\text{Ta}^{\text{V}}/\text{Ta}^{\text{III}}$ cycle involving reductive elimination of hydrogen from Cp_2TaH_3 (or from an isotopologue) to generate Cp_2TaH followed by reversible oxidative addition of an arene C–H bond into Cp_2TaH to form $\text{Cp}_2\text{TaH}_2\text{Ar}$ (Scheme 1). The involvement of Ta^{III} in the H/D exchange process was supported by Rausch and Atwood's 1982 report, which showed that the same process can occur under low-temperature photochemical conditions.^{16e} They observed H_2 , together with HD and D_2 , upon photolysis of Cp_2TaH_3 in C_6D_6 . The presence of H_2 in the reaction mixture is consistent with its reductive elimination from Cp_2TaH_3 . Furthermore, the Ta^{III} complex $\text{Cp}_2\text{Ta}(\text{CO})\text{H}$ was also found to catalyze photoinduced H/D exchange between arenes and hydrogen.^{16e}

Density Functional Theory Calculations on the Benzene Activation Mechanism. We conducted density functional theory (DFT) calculations to investigate the mechanism of benzene activation by Cp_2TaH_3 . Geometry optimizations were performed with the M06L¹⁷ functional, the 6-31+G(d,p) basis set for carbon and hydrogen, and the LANL2DZ pseudopotential for tantalum (referred to herein as basis set 1, BS1). Energies of optimized structures were further refined at the CPCM (benzene or toluene)-M06¹⁸/6-311++G(2d,p)/SDD(Ta) level of theory (M06/BS2, see Computational Section for further details). The Minnesota functionals M06L and M06 were selected on the basis of prior benchmarking studies with transition metals.^{17–19} We first considered the $\text{Ta}^{\text{V}}/\text{Ta}^{\text{III}}$ pathway that had been proposed in the 1970s (Scheme 2).

This pathway is initiated by the endergonic reductive elimination of H_2 from Cp_2TaH_3 (1) to provide Cp_2TaH (2). At the level of theory used and with most other functionals that we evaluated (see Supporting Information), this Ta^{III} complex is predicted to be more stable in the triplet electron

configuration ($S = 1, ^3\text{2}$) than as a singlet ($S = 0, ^1\text{2}$).^{12,14,20} Interestingly, some prior DFT studies on silica-supported Ta^{III} monohydrides predicted that the closed shell singlet is the more stable ground-state configuration.¹² The discrepancy between our calculations on Cp₂TaH and those on a silica-supported analogue appears to be a consequence of the supporting ligand structures used, rather than resulting from the DFT method choice (see Supporting Information).^{20c} However, DFT has known limitations to making accurate predictions about electronic configurations, and different methods can be biased toward favoring either high or low spin states (see Supporting Information).²¹

On both the triplet and singlet potential energy surface, loss of H₂ is barrierless at the M06L/BS1 level of theory. Specifically, no energy maximum is detected in a relaxed scan of the potential energy along the reaction coordinate for H–H bond formation from Cp₂TaH₃ (see Supporting Information). The absence of a detectable energy maximum suggests that any activation energy associated with H₂ reductive elimination corresponds to an entropic barrier and is likely very small.^{22,23}

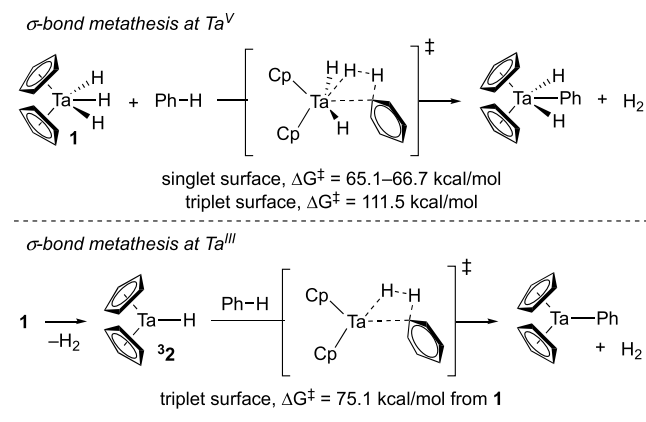
Although high spin ³2 is calculated to be more stable than low spin ¹2, the energetics of subsequent steps on the triplet energy surface are unreasonably high, suggesting that the catalytic reaction occurs on the singlet energy surface. Complex ¹2 can interact with benzene to form π -complex **3**. No such π -complex can be located with spin = 1. Indeed, the Dewar–Chatt–Duncanson model for π -complexation (see Supporting Information) gives tantalum d⁰ (Ta^V) character, which would preclude location of spin density on tantalum. On the singlet energy surface, π -complexation is exergonic relative to ¹2. Interestingly, the predicted favorability of π -complexation is method-dependent (see Supporting Information). Other dispersion-containing methods (e.g., B3LYP-D3) also predict that the π -complex is more stable than ¹2; however, this step is predicted to be endergonic with methods that do not include dispersion (e.g., B3LYP). The difference in predictions with and without dispersion suggests that stabilization of the π -complex can largely be attributed to attractive London dispersion interactions. Notably, even when dispersion is included, the π -complex has considerably higher energy than the starting Ta^V trihydride. However, low concentrations of H₂ and high concentrations of arenes could promote the formation of **3** under experimental conditions.

From the π -complex, oxidative addition of an aromatic C–H bond is predicted to proceed through a barrier of about 12–14 kcal/mol measured from the high-energy intermediate **3**. Two low-spin transition structures were located with nearly identical energies: one involving C–H activation to place Ph at an internal position (¹TS4 resulting in **6**) and the other placing Ph at the lateral position (¹TS5 resulting in **7**). Overall, the activation barrier to C–H activation through either transition structure is about 33 kcal/mol, as measured from **1**.

On the triplet energy surface, an oxidative addition transition structure placing phenyl at the internal position (³TS4) is predicted to be prohibitively high in energy, and an oxidative addition transition structure that places phenyl at a lateral position could not be located. These results indicate that tantalum has too much Ta^V/d⁰ character during reaction with benzene for triplet transition states to be energetically accessible. As such, although both ¹2 and ³2 are likely formed, only ¹2 lies on a productive pathway to benzene activation.

We also considered σ -bond metathesis mechanisms for C–H activation (Scheme 3). σ -Bond metathesis is a common

Scheme 3. σ -Bond Metathesis Mechanisms for Benzene C–H Activation Are Predicted to be Prohibitively High Energy



elementary reaction of d⁰ metals,^{6c} and this type of pathway was previously proposed for C–H activation of butane at silica-supported Ta^V trihydrides.^{12,20c} Several transition structures for benzene activation by σ -bond metathesis at both Cp₂TaH₃ and Cp₂TaH were located on the singlet and triplet potential energy surfaces, respectively. However, all of the transition structures that we located are predicted to be very high energy (65–112 kcal/mol relative to **1**; see Supporting Information). As such, our calculations suggest that C–H activation is more likely to proceed through oxidative addition at Ta^{III} than by σ -bond metathesis.²⁴

Thermal H/D Exchange between Cp₂TaH₃ and C₆D₆

As described above, H/D exchange between Cp₂TaH₃ and deuterated benzene has been previously reported.^{16a,e} We first sought to reproduce this observation in order to establish a baseline for comparison to H/D exchange under different conditions, using other hydrocarbons, or with other tantalum hydrides.

Cp₂TaH₃ was prepared through a three-step route previously reported by Nikonov et al.²⁵ In our hands, this route yields Cp₂TaH₃ as a white solid that retains its color even after storage for 12 months under nitrogen. In contrast, our efforts to employ an alternative one-pot route^{16d} led to a product that takes on a pink-to-red impurity within 14 days of storage. This impurity is NMR-silent²⁶ and can only be removed by repeated sublimations. As such, Nikonov's three-step route to Cp₂TaH₃ is preferred.

In an initial experiment, Cp₂TaH₃ (0.012 mmol) was combined with C₆D₆ (~500 equiv) and cyclohexane (NMR internal standard, 1 equiv) in a medium wall high-pressure sealed NMR tube (9" length, 3.46 mm internal diameter) under N₂ (60 psi).²⁷ Consistent with previous reports,^{16c,d,26b} the hydride signals of Cp₂TaH₃ display an AB₂ pattern in the upfield region of the ¹H NMR spectrum (Figure 1A). The protons of the Cp rings appear as a singlet at 4.76 ppm (see Supporting Information). The internal hydride appears as a triplet at –1.61 ppm, while the two lateral hydrides are represented by a doublet at –3.01 ppm. After heating at 100 °C for 1 h, new hydride signals were detected, assigned to the partially deuterated analogues of Cp₂TaH₃ (Figure 1B). The internal hydride of monodeuterated **1-d₁a** is shifted upfield by 51 ppb and appears as a broad doublet (the ¹H–D coupling

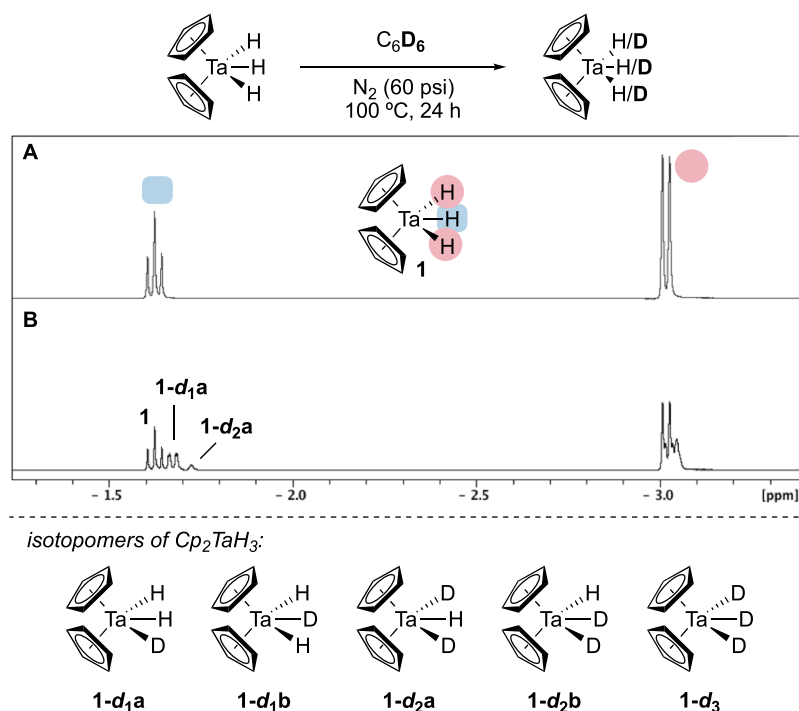


Figure 1. Hydride region of the ^1H NMR spectrum of Cp_2TaH_3 (A) before and (B) after heating for 1 h in the presence of C_6D_6 . Acquired on a 500 MHz instrument.

constant is too small for the signal to be resolved into a doublet of 1:1:1 triplets). The internal hydride of dideuterated $1\text{-d}_2\text{a}$ is shifted upfield by 99 ppb relative to Cp_2TaH_3 and appears as a broad singlet. The lateral hydride signals of the various mono- and dideuterated isotopologues overlap each other. There is no change in the appearance of the Cp signal at 4.76 ppm, suggesting that H/D exchange does not take place on this ligand.^{16d} However, it is unknown whether isomers containing deuterated Cp rings would be resolved by NMR.

In subsequent experiments, the rates of H/D exchange were quantified by monitoring reactions over a period of at least 6 h. ^1H NMR spectra were acquired approximately once per hour. In each spectrum, the integrations of the internal and lateral hydride signals from all observed isotopologues were summed together (the regions from -1.58 to -1.75 and from -2.98 to -3.01 ppm shown in Figure 1B, represented by the term “[hydride]” below). The change in [hydride] over time is thus the negative of the uncorrected rate of H/D exchange

$$r_{\text{uncorr}} = - \frac{d[\text{hydride}]}{dt}$$

However, it is possible that some of the disappearance in hydride signals could be due to other decomposition pathways for Cp_2TaH_3 . To account for this, the extent of Cp_2TaH_3 decomposition was quantified by measuring the decrease in Cp signal integration relative to the cyclohexane internal standard (this approach assumes that erosion of the Cp signal is not due to deuteration at Cp).

$$r_{\text{decomp}} = - \frac{d[\text{Cp}]}{dt}$$

Finally, the rate of H/D exchange was corrected to account for decomposition of the tantalum complex. The corrected observed rate, denoted as r_{corr} is thus described by the following equation

$$r_{\text{corr}} = r_{\text{uncorr}} - r_{\text{decomp}}$$

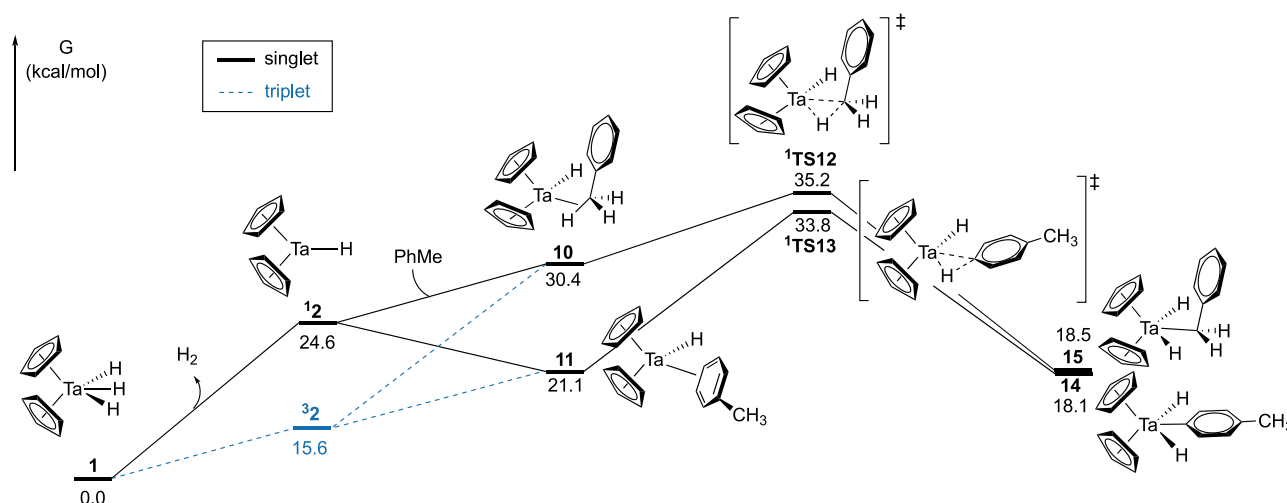
As shown in Table 1 entry 1, the rate of H/D exchange under the conditions described above is about 5X the rate of decomposition.

The extent of unproductive decomposition poses a severe barrier to the future development of Cp_2TaH_3 as a catalyst for hydrocarbon activation. However, we have found that the behavior of Cp_2TaH_3 is affected by its starting purity. In particular, although sublimation of Cp_2TaH_3 does not change

Table 1. Rate of Tantalocene Decomposition and H/D Exchange with C_6D_6 ^a

entry	complex	conditions ^b	r_{decomp}^c	r_{corr}^d	r_{rel}^e
1	1	Δ , N_2	5.16(34)	23.95(93)	1.00
2 ^f	1	Δ , N_2	5.57(61)	24.28(240)	1.01
3	1	$h\nu$, N_2	4.61(26)	16.85(59)	0.70
4	1	Δ , D_2	3.78(163)	1.63(30)	0.07
5	1	$h\nu$, D_2	2.77(18)	7.01(16)	0.29
6	8	Δ , N_2	1.11(22)	4.84(60)	0.20
7	9	Δ , N_2	0.00	0.00	0.00

^aAll experiments were performed in triplicate, and the results are an average of the collected data. Uncertainties in r_{decomp} and r_{corr} values are reported in parentheses. Reactions were followed for 6 h. ^b Δ signifies heating at 100°C , $h\nu$ signifies irradiation at 350 nm at 35°C ; and N_2 and D_2 = atmosphere pressurized to 60 psi. ^c r_{decomp} describes the rate of catalyst decomposition, in units of $\text{M} \times \text{h}^{-1} \times 10^{-7}$. ^d r_{corr} describes the rate of catalytic H/D exchange following correction accounting for decomposition, in units of $\text{M} \times \text{h}^{-1} \times 10^{-7}$. ^e r_{rel} describes relative values of r_{corr} with respect to those in entry 1 ^fTantalocene not sublimed prior to experiments.

Scheme 4. Calculated Pathways for the Reaction of Cp_2TaH_3 with Toluene via an Oxidative Addition Mechanism for Aromatic or Benzylic C–H Activation

the appearance of its ^1H NMR spectrum, it leaves behind a quantity of off-white solids that display poor solubility in aromatic solvents. Apparently, sublimation separates Cp_2TaH_3 from NMR silent impurities (likely tantalum oxides). Although similar average rates of decomposition and H/D exchange are observed for the sublimed and unsublimed materials (Table 1 compare entries 1 and 2), variability in rate data is appreciably higher for the unsublimed complex.

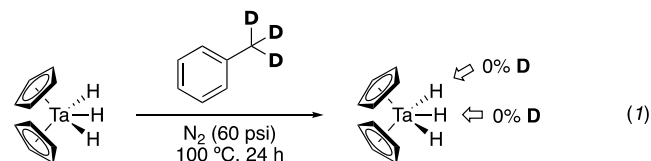
Comparison of Thermal and Photochemical Conditions for H/D Exchange. H/D exchange between benzene and D_2 catalyzed by Cp_2TaH_3 has also been reported under low-temperature photochemical conditions.^{16c} However, these conditions had not been directly compared to the thermal conditions. In order to evaluate the relative efficiency of thermal and photochemical conditions, we conducted photochemical H/D exchange studies analogous to those described in the section above. Cp_2TaH_3 (0.012 mmol) was combined with C_6D_6 (~500 equiv) and cyclohexane (NMR internal standard, 1 equiv) in a medium wall high-pressure sealed NMR tube (9" length, 3.46 mm internal diameter) under N_2 (60 psi).²⁷ The reaction mixture was irradiated with 350 nm light at a constant temperature of 35 °C.^{28,29} Under these conditions, the rate of H/D exchange is moderately slower than the thermal conditions at 100 °C (compare entries 1 and 3 of Table 1). The rate of catalyst decomposition under thermal and photochemical conditions is similar. However, whereas the reaction mixture remains colorless during thermal H/D exchange, the photochemical conditions induce a deep red color that persists for several hours upon removal from the light source.³⁰

In contrast to our photochemical studies under N_2 , prior literature reports described both thermal and photochemical reactions of Cp_2TaH_3 with protio-arenes under a D_2 atmosphere.¹⁶ Furthermore, preparation of Cp_2TaD_3 has been described by an H/D exchange process involving heating Cp_2TaH_3 in C_6D_6 under D_2 .³¹ Interestingly, we observed that deuterium incorporation at Ta is actually slower under an atmosphere of D_2 compared to an equivalent initial pressure of N_2 , at least in our NMR-scale experiments that allow for only a small headspace volume. This phenomenon is observed under both thermal (Table 1 entry 4) and photochemical conditions (entry 5), although it is more pronounced under the thermal

conditions. This result is surprising because capture of the Ta^{III} intermediate Cp_2TaH by D_2 is expected to be fast and would lead to deuteration of tantalum. The attenuated rate of H/D exchange at Ta under D_2 may suggest that (1) reductive elimination of H_2 from Cp_2TaH_3 is kinetically inhibited under an atmosphere of D_2 or (2) dissociation of H_2 from a putative $\text{Cp}_2\text{TaH}(\text{H}_2)$ intermediate (not located computationally) is slower under D_2 pressure, thereby more strongly favoring the Cp_2TaH_3 resting state.

Overall, the results suggest that H/D exchange between Cp_2TaH_3 and C_6D_6 is moderately faster at 100 °C than under photochemical conditions at 30 °C. Furthermore, at the reaction volume investigated, deuterated isotopologues of Cp_2TaH_3 are formed faster under an atmosphere of N_2 (60 psi), where the only deuterium source is C_6D_6 , than under an equivalent pressure of D_2 .

Activation of Toluene. We next turned to understanding the lack of reactivity of benzylic C–H bonds toward activation by Cp_2TaH_3 . In previously described studies of the reaction between Cp_2TaH_3 and toluene in the presence of D_2 , H/D exchange was reported to occur only at the aromatic positions, with no deuterium incorporation at the benzylic site.^{16d} We reproduced this result (see Supporting Information) and also conducted the complementary experiment shown in eq 1. In this experiment, Cp_2TaH_3 was reacted with toluene- $\alpha,\alpha,\alpha\text{-d}_3$. No deuterium incorporation at tantalum was detected by NMR after 24 h at 100 °C.



The lack of reactivity of a weak benzylic C–H site is potentially discouraging toward the possibility of using homogeneous tantalum complexes for activating aliphatic hydrocarbons. However, we reasoned that understanding the poor reactivity of the benzylic position might provide insights into whether this limitation might be overcome.

Interestingly, DFT calculations suggest that the barrier to oxidative addition of a benzylic C–H bond of toluene at Cp_2TaH is comparable to the barrier for reaction of an

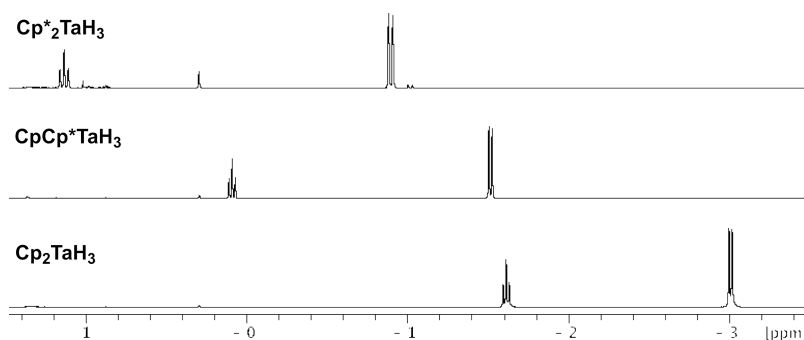
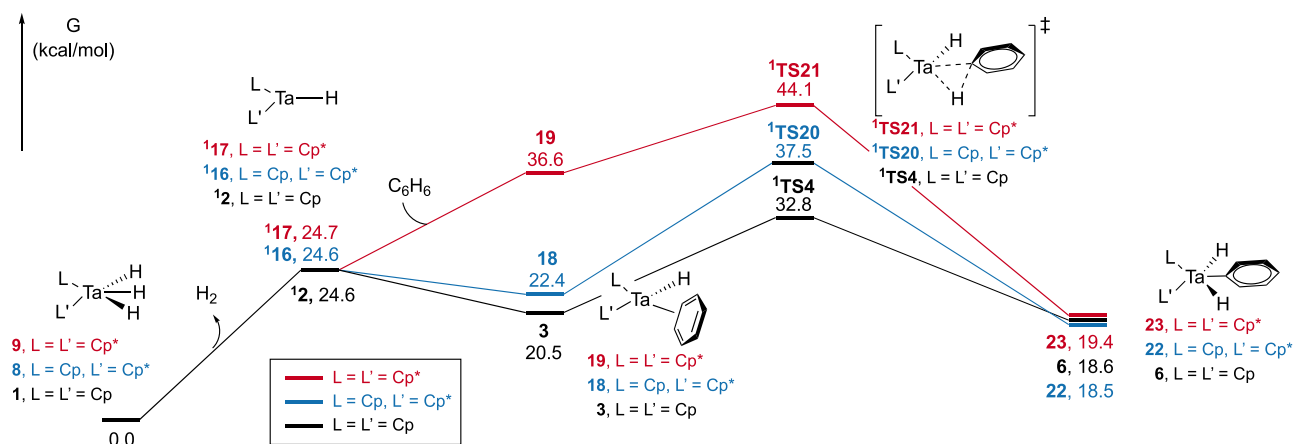


Figure 2. Comparison of the hydride regions of the ^1H NMR spectra of $\text{Cp}^*_2\text{TaH}_3$, $\text{CpCp}^*\text{TaH}_3$, and Cp_2TaH_3 .

Scheme 5. Comparison of Calculated Free Energy Surfaces for the Reaction of Cp_2TaH_3 and Permethylated Analogues with Benzene via an Oxidative Addition Mechanism



aromatic C–H bond (compare $^1\text{TS12}$ and $^1\text{TS13}$, Scheme 4, and see Supporting Information for other higher energy transition structures). σ -Bond metathesis transition structures for benzylic C–H activation were also located, but their energies are much higher than the oxidative addition mechanism (see Supporting Information). Despite the similarity between the predicted barriers to benzylic and aromatic C–H activation, a key difference between the reaction at the two sites is the energy of the complex immediately preceding oxidative addition. Formation of a π -complex (**11**) is exergonic from **12** and precedes oxidative addition of an aromatic C–H bond. In contrast, the σ -complex (**10**) that precedes benzylic C–H activation is high energy. Similar to π -complexation, a σ -complex could only be located on the singlet energy surface. As such, the π -complex is expected to exist in much higher concentration than the σ -complex under the reaction conditions, which enables aromatic C–H activation to outcompete benzylic activation. Arene π -complexation to coordinatively unsaturated metal centers is typically stabilizing, and is known to often precede and direct C–H activation.^{32,33}

Importantly, the similar calculated ΔG^\ddagger values for reaction at aromatic and benzylic C–H bonds suggest that oxidative addition of $\text{C}_{(\text{sp}^3)}\text{--H}$ bonds at Ta^{III} may yet be feasible in the absence of competing aromatic bonds. Starting from a tantalocene hydride like Cp_2TaH_3 , aliphatic C–H activation would be most likely to succeed under conditions where H_2 is removed from reaction to drive conversion of Cp_2TaH_3 to Cp_2TaH .

H/D Exchange between $\text{CpCp}^*\text{TaH}_3/\text{Cp}^*_2\text{TaH}_3$ and C_6D_6 . Because the data suggest that Cp_2TaH_3 decomposes at a significant rate even under the optimal thermal conditions, we were interested in considering permethylated analogues of this compound. These analogues have been reported to be more stable and to have better solubility properties than Cp_2TaH_3 .³⁴ However, to our knowledge, neither $\text{Cp}^*_2\text{TaH}_3$ nor $\text{Cp}^*\text{CpTaH}_3$ have been investigated for their ability to activate C–H bonds ($\text{Cp}^* = \eta^5\text{-C}_5\text{Me}_5$).

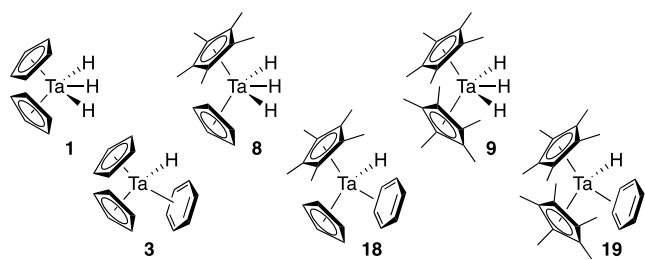
$\text{Cp}^*_2\text{TaH}_3$ and $\text{Cp}^*\text{CpTaH}_3$ were prepared through previously described divergent routes that involve common intermediates.^{26c,34f} Like Cp_2TaH_3 , both permethylated analogues exhibit an AB_2 splitting pattern in the hydride region of their ^1H NMR spectra (Figure 2). The hydride signals are shifted downfield with increasing methylation on the cyclopentadienyl rings.³⁵

The possibility for the permethylated complexes to activate benzene was investigated. When $\text{CpCp}^*\text{TaH}_3$ was heated to 100°C in C_6D_6 under a N_2 atmosphere, H/D exchange was observed based on the change in the hydride signals of the ^1H NMR spectrum. Furthermore, as expected, this complex displays greater stability toward decomposition than the parent complex Cp_2TaH_3 : the decomposition rate of $\text{CpCp}^*\text{TaH}_3$ is about one-fifth of that of Cp_2TaH_3 (Table 1, entry 6). Increased catalyst stability has been noted previously upon permethylation of cyclopentadienyl ligands³⁴ due to preclusion of a ring α -hydrogen shift^{34c} (possibly via an $\eta^5\text{--}\eta^1$ hapticity slip).³⁶ However, the pentamethyl complex is also less active toward benzene activation; the rate of deuterium incorporation at tantalum is $5\times$ slower than that observed for Cp_2TaH_3 .

In keeping with a trend that permethylation increases stability while decreasing reactivity toward C–H activation, no reaction was observed with $\text{Cp}_2^*\text{TaH}_3$. Under the conditions in Table 1, this complex neither reacts with C_6D_6 nor decomposes through other routes under the applied conditions (entry 7).³⁷

To better understand the decreased catalytic activity of the permethylated complexes, we conducted DFT calculations on benzene activation with $\text{CpCp}^*\text{TaH}_3$ (**8**) and $\text{Cp}_2^*\text{TaH}_3$ (**9**). Scheme 5 compares the resulting energy values to those of the corresponding reaction using Cp_2TaH_3 . Although reductive elimination of H_2 remains barrierless at this level of theory for both $\text{CpCp}^*\text{TaH}_3$ and $\text{Cp}_2^*\text{TaH}_3$, the activation barriers for oxidative addition of Ph-H at Ta^{III} are higher with increased methylation of the ligands (compare structures ¹TS4, ¹TS20, and ¹TS21). These results are consistent with a steric argument for the decreased reactivity of permethylated tantalocene hydrides and qualitatively match our experimental observations. Furthermore, in contrast to the results with the unmethylated and the pentamethylated complex, formation of a π -complex between Cp_2^*TaH and benzene (**19**) is no longer stabilizing relative to low spin Cp_2TaH . The rationale for this observation appears to be sterics; π -coordination of benzene to Cp_2^*TaH leads to greater distortion of the $[\text{Cp}_2^*\text{Ta}]$ geometry than observed in the analogous reaction of Cp_2TaH or $\text{CpCp}^*\text{TaH}_3$. Table 2 compares the calculated geometries of

Table 2. Calculated Geometric Parameters for $\text{LL}'\text{TaH}_3$ and the Corresponding Benzene π -Complexes



L	L'	complex	Ta–L ^a	$\Delta\text{Ta–L}^b$	$\angle\text{L/L}'^c$	$\Delta\angle\text{L/L}'^d$
Cp	Cp	1	2.065	–0.005	36.2	9.7
		3	2.060		45.9	
Cp	Cp*	8	2.072	0.008	38.0	8.6
		18	2.080		46.6	
Cp*	Cp*	9	2.088	0.046	30.9	14.5
		19	2.134		45.4	

^aAverage distance (in Å) between Ta and cyclopentadienyl ligand centroids. ^bChange in the average distance between Ta and L/L' centroids upon conversion of $\text{LL}'\text{TaH}_3$ to the corresponding π -complex. ^cAngle between cyclopentadienyl planes (in degrees). ^dChange in the angle between cyclopentadienyl planes upon conversion of $\text{LL}'\text{TaH}_3$ to the corresponding π -complex.

the π -complexes to their corresponding Ta^{V} trihydride precursors. If the Ta^{V} trihydrides are assumed to have “ideal” bent sandwich geometries³⁸ (an assumption based on their experimental stability), increased deviation from these geometries upon formation of a π -complex is consistent with decreased stability of the π -complex. Indeed, the angle between cyclopentadienyl planes in π -complexes **3** and **18** is only $\sim 9^\circ$ larger than in the corresponding Ta^{V} trihydrides. However, this angle increases by almost 15° in π -complex **19** compared to $\text{Cp}_2^*\text{TaH}_3$. Additionally, the average distance between Ta and

the Cp^* ring centroid increases by 0.05 Å in π -complex **19**, whereas the change in this parameter is negligible in the unmethylated or pentamethylated π -complexes **3** and **18**. The increased distortion of the decamethylated π -complex **19** compared to $\text{Cp}_2^*\text{TaH}_3$ reflects the steric demand on the methyl groups in order to accommodate an incoming arene.

Taken together, the experimental and computational data suggest that the increased stability of the permethylated tantalocene hydrides is counterbalanced by lower catalytic activity. The increased steric demand of Cp^* ligands, compared to Cp, raises the energy of the π -complexes and of the oxidative addition transition structures.

CONCLUSIONS

This work addressed several fundamental questions about the reaction of tantalocene hydrides with arenes. These questions were presented in the Introduction, and our findings are summarized below.

1. What is the mechanism of C–H activation by Cp_2TaH_3 ?

Our DFT calculations strongly support an oxidative addition mechanism for arene activation, rather than a σ -bond metathesis mechanism. The favored mechanism involves reductive elimination of H_2 to provide $\text{Cp}_2\text{Ta}^{\text{III}}\text{H}$, which is oxidized back to Ta^{V} upon reaction with a C–H bond. Although $\text{Cp}_2\text{Ta}^{\text{III}}\text{H}$ is predicted to be more stable in a high-spin (triplet) electron configuration, its reaction with arenes appears to take place on the singlet energy surface.

2. How do thermal versus photochemical conditions compare for arene C–H activation?

Reaction of Cp_2TaH_3 with C_6D_6 can occur under thermal conditions (100 °C) or photochemical conditions (35 °C, 350 nm). H/D exchange is moderately faster under the thermal conditions ($r_{\text{rel}} = 1.0$ for thermal vs 0.7 for photochemical). The difference in the rate of catalyst decomposition is approximately proportional to the difference in the H/D exchange rate. As such, the photochemical conditions do not offer any particular advantage for H/D exchange with benzene unless low temperatures are deemed desirable.

3. Why are benzylic $\text{C}_{(\text{sp}^3)}\text{H}$ bonds unreactive toward activation by Cp_2TaH_3 ?

DFT calculations suggest that the barrier to activation of a benzylic C–H bond is only slightly higher than the barrier for activation of an aromatic C–H bond. However, formation of a π -complex between toluene and Cp_2TaH is exergonic, whereas a σ -complex between Cp_2TaH and a benzylic C–H bond is endergonic. The stable π -complex likely directs C–H activation at an aromatic C–H bond, such that aromatic C–H activation outcompetes benzylic activation. Activation of aliphatic hydrocarbons may be feasible in the absence of π -coordinating arenes.

4. How does the reactivity of more readily handled permethylated tantalocene hydrides ($\text{CpCp}^*\text{TaH}_3$ and $\text{Cp}_2^*\text{TaH}_3$, where $\text{Cp}^* = \eta^5\text{-C}_5\text{Me}_5$) compare to that of Cp_2TaH_3 ?

The penta- and decamethylated analogues of Cp_2TaH_3 are more stable than Cp_2TaH_3 , as evidenced by a slower rate of decomposition upon heating in C_6D_6 . However, their slower decomposition is counterbalanced by a correspondingly slower rate of H/D exchange with C_6D_6 . In fact, $\text{Cp}_2^*\text{TaH}_3$ displays no catalytic activity (nor decomposition) at all upon heating in

C_6D_6 at 100 °C for several hours. The results of DFT calculations are consistent with a steric explanation for the lack of reactivity of $Cp_2^*TaH_3$. In particular, the $[Cp_2^*Ta]$ framework undergoes more extensive unfavorable distortion upon π -coordination compared to the corresponding $[Cp_2Ta]$ or $[CpCp^*Ta]$ scaffolds.

The use of early transition metals for hydrocarbon activation is attractive because of their high reactivity toward inert bonds. Although homogeneous tantalum hydrides are potential candidates for catalytic hydrocarbon upgrading, strategies to enhance the stability of such complexes without detracting from their activity will be necessary in order to realize their potential as C–H activation catalysts. Furthermore, activation of $C_{(sp^3)}-H$ bonds by homogeneous tantalocene hydrides remains elusive.

■ EXPERIMENTAL SECTION

General Materials and Methods. Sodium bis(trimethylsilyl)-amide and *tert*-butylamine were obtained from Acros Organics and used as received. Methyl iodide and pyridine were obtained from Acros Organics in ACROSeal bottles and used as received. Dicyclopentadiene was obtained from Acros Organics and passed across a short silica plug to remove water and stabilizer prior to use. Sodium metal (foil-wrapped sticks in mineral oil) was obtained from Acros Organics and washed with copious hexanes prior to use. $TaCl_5$ was obtained from Acros Organics and purified by sublimation prior to use. Di-*n*-butyl ether, sodium metasilicate, and triphenyl phosphite were obtained from Alfa Aesar and used as received. Potassium hydride (30% w/w in mineral oil) was obtained from Alfa Aesar, washed with copious hexanes, and then dried under high vacuum before use. Isotopically labeled compounds (C_6D_6 , $CDCl_3$, D_2 , DMSO- d_6 , and toluene- $\alpha,\alpha,\alpha-d_3$) were obtained from Cambridge Isotopes. Dichloromethane, diethyl ether (Et_2O), pentane, tetrahydrofuran (THF), and toluene were obtained from Fisher Chemical, degassed, and dried on a JC Meyer solvent system prior to use. Magnesium turnings and tri-*n*-butyltin chloride were obtained from Oakwood Chemical and used as received. Trimethylphosphine was either prepared according to a procedure adapted from the literature (*vide infra*)³⁹ or purchased from Strem and used as received. 1,2,3,4,5-Pentamethylcyclopentadiene and lithium aluminum hydride were obtained from TCI America and used as received. Unless otherwise noted, all operations were performed in a nitrogen-filled glovebox or using air-free techniques in oven-dried glassware. NMR spectra were recorded at 298 K on a Bruker DRX 500 MHz (500.233 MHz for 1H) spectrometer. Elevated-pressure 1H NMR experiments were performed in 9 in. Wilmad Glass medium-wall high-pressure precision NMR tubes. 1H NMR chemical shifts are reported in parts per million (ppm) relative to TMS, with the residual solvent peak used as an internal reference [$CHCl_3$ (7.26 ppm), C_6D_5H (7.16 ppm), and DMSO- d_5 (2.50 ppm)].

General Procedure for Measuring H/D Exchange Rates by 1H NMR. In a 4 mL vial within a glovebox, tantalocene trihydride (0.2 mol % relative to arene) was fully dissolved in a solution of deuterated arene (1.80 mL) containing cyclohexane (0.2 mol % relative to arene). The resulting solution was divided equally (0.60 mL each) into three medium-wall high-pressure precision NMR tubes (Wilmad, 9" length, 3.46 mm internal diameter), and the tubes were sealed with Teflon stopcocks and removed from the glovebox. One at a time, the tubes were connected to a Schlenk line and pressurized to 60 psi (4.14 bar) with the desired gas. In experiments using H_2 or D_2 , the tube was immersed in liquid nitrogen until the contents were frozen (about 1 min) and then evacuated and refilled three times with the desired gas, sealed, and warmed to room temperature in a water bath (about 2 min). In experiments using a nitrogen atmosphere, low-temperature evacuation–refill cycles were unnecessary as the headspace of the tube was already filled with nitrogen from the glovebox.⁴⁰ Initial 1H NMR spectra (500 MHz, 32 scans, D1 relaxation delay = 10 s) were obtained of each sample (time = 0 h), and the samples were heated in

a Chemglass NMR tube reaction heating block or irradiated at 350 nm in a Rayonet RPR-1000 photochemical reactor for a total of 6 h (not including breaks for acquiring NMR spectra). NMR spectra were acquired approximately every hour (exact times were recorded and used during analysis of the results). During processing, the integration values of all signals were standardized relative to the cyclohexane signal (the cyclohexane signal integration was set to 10). Integration values were then normalized by multiplying the integral by a scalar value to correct for the actual initial concentrations at $t = 0$.

Synthesis of $NaCp-1/3$ THF (24). The title compound was prepared according to a procedure adapted from the literature.⁴¹ Sodium (2.00 g, 87.0 mmol) was added to dicyclopentadiene (160 mL), and the mixture was heated at 160 °C for 24 h until hydrogen evolution ceased and no sodium remained. The copious white solid was collected by vacuum filtration. This solid was heated in toluene (60 mL) and THF (6 mL) at reflux for 1 h, after which it was collected by vacuum filtration, washed with copious pentane, and dried *in vacuo* to give a free-flowing off-white solid (6.78 g, 60.5 mmol, 69% yield). Spectral data are consistent with those previously reported.⁴¹

Synthesis of $Ta(=NCMe_3)Cl_3(py)_2$ (25). The title compound was prepared according to a procedure adapted from the literature.^{25c} *tert*-Butylamine (5.9 mL, 56 mmol) and pyridine (20.0 mL, 250 mmol) were added sequentially to a stirred heterogeneous mixture of freshly sublimed $TaCl_5$ (10.00 g, 27.9 mmol) and Na_2SiO_3 (6.84 g, 56.0 mmol) in toluene (80 mL) and Et_2O (20 mL). The mixture was stirred for 18 h, after which it was filtered over Celite. The Celite plug was washed with toluene, and the combined filtrates were concentrated *in vacuo* to give an opaque yellow solid. Recrystallization from dichloromethane/pentane at –25 °C gave large yellow crystals after 5 d (8.04 g, 56% yield). An additional product can be obtained from the same recrystallization liquor with additional time and pentane additions. Spectral data are consistent with those previously reported.^{25c}

Synthesis of $Cp_2Ta(=NCMe_3)Cl$ (26). The title compound was prepared according to a procedure adapted from the literature.^{25b} While cooling to –84 °C,⁴² a solution of $NaCp-1/3$ THF (1.88 g, 16.88 mmol, 2.1 equiv) in Et_2O (60 mL) and THF (15 mL) was added to a heterogeneous solution of $Ta(=NCMe_3)Cl_3(py)_2$ (4.13 g, 8.00 mmol, 1.0 equiv) in Et_2O (270 mL). The mixture was allowed to slowly warm to room temperature and stirred for 18 h, after which solvent removal *in vacuo* gave an opaque red solid. Extraction into pentane (3 × 50 mL) and concentration of the combined extracts gave a deep red oily-to-waxy product (2.79 g, 83% yield). Spectral data are consistent with those previously reported.^{25b}

Synthesis of Cp_2TaH_3 (1). The title compound was prepared according to a procedure adapted from the literature.^{25a} While cooling to –84 °C, a solution of $Cp_2Ta(=NCMe_3)Cl$ (2.79 g, 6.68 mmol, 1.0 equiv) in Et_2O (65 mL) was added to a suspension of $LiAlH_4$ (1.02 g, 26.8 mmol, 4.0 equiv) in Et_2O (65 mL). The mixture was allowed to slowly warm to room temperature and stirred for 18 h, after which it was cooled to 0 °C and degassed deionized water was added dropwise (1.96 mL, 108 mmol, 16 equiv). Extraction of the mixture into Et_2O (3 × 50 mL) and concentration of the combined extracts gave an off-white solid (0.90 g, 43% yield). Spectral data are consistent with those previously reported.^{25a}

Synthesis of $NaCp^*$ (27). The title compound was prepared according to a procedure adapted from the literature.⁴³ 1,2,3,4,5-Pentamethylcyclopentadiene (7.43 g, 54.6 mmol, 1.0 equiv) was added dropwise to a stirred solution of sodium bis(trimethylsilyl)-amide (9.17 g, 50.0 mmol, 0.92 equiv) in Et_2O (45 mL), and the opaque suspension was allowed to stir for 18 h. After this time, the solid product was collected by vacuum filtration, washed with Et_2O (2 × 5 mL) and pentane (2 × 10 mL), and dried *in vacuo* to give a white solid (5.69 g, 40.0 mmol, 72% yield). Spectral data are consistent with those previously reported.⁴³

Synthesis of $(n-Bu)_3SnCp^*$ (28). The title compound was prepared according to a procedure adapted from the literature.⁴⁴ $(n-Bu)_3SnCl$ (9.0 mL, 33.2 mmol, 1.0 equiv) was added dropwise to a stirred suspension of $NaCp^*$ (5.25 g, 33.2 mmol, 1.0 equiv) in toluene (200

mL), rapidly yielding a change from a colorless opaque suspension to a pale yellow translucent solution. The mixture was stirred for 2 days at room temperature, after which it was filtered across Celite and washed with copious toluene, and the combined filtrates concentrated *in vacuo* to give a pale yellow oil (13.24 g, 31.1 mmol, 94% yield). Spectral data are consistent with those previously reported.⁴⁴

Synthesis of Cp*TaCl₄. The title compound was prepared according to a procedure adapted from the literature.⁴⁴ (*n*-Bu)₃SnCp* (13.24 g, 31.14 mmol, 1.2 equiv) was added to a suspension of freshly sublimed TaCl₅ (9.40 g, 26.25 mmol, 1.0 equiv) in toluene (110 mL), resulting in the immediate formation of a fine yellow solid. The suspension was allowed to stir for 24 h, after which the solid was collected by vacuum filtration, washed with pentane (3 × 10 mL), and dried under vacuum to give a free-flowing yellow powder (11.32 g, 24.6 mmol, 94% yield) that was used without further purification.

Synthesis of PMe₃ (29). The title compound was prepared according to a procedure adapted from the literature.³⁹ Dibutyl ether (200 mL) was added to iodine-activated Mg turnings (11.68 g, 480.5 mmol), and methyl iodide (23.5 mL, 377.5 mmol, 1 equiv) was then added slowly, taking care to avoid an excessively exothermic reaction upon initiation of the Grignard formation. After the addition of methyl iodide, the mixture was cautiously brought to reflux for 24 h and then allowed to cool to room temperature. The solution was decanted from the remaining magnesium by cannula transfer, and a solution of triphenyl phosphite (27.0 mL, 310.3 mmol, 0.8 equiv) in dibutyl ether (40 mL) was added slowly with cooling to 0 °C. The mixture was then heated to 40 °C for 3 h, after which the product was obtained as a pure, colorless liquid by distillation (6.0 mL, 58.2 mmol, 57% yield). Spectral data are consistent with those previously reported.³⁹

Synthesis of Cp*TaCl₃(PMe₃). The title compound was prepared according to a procedure adapted from the literature.^{26c} While cooling to -84 °C, THF (50 mL) was transferred to a flask containing Cp*TaCl₄ (7.27 g, 15.9 mmol, 1.0 equiv) and magnesium turnings (0.19 g, 7.9 mmol, 0.5 equiv), followed by the addition of a solution of PMe₃ (1.72 mL, 16.9 mmol, 1.1 equiv) in THF (5 mL). The reaction mixture was allowed to slowly warm to room temperature, during which the mixture changed from a yellow suspension to a deep-red solution. After stirring for 24 h, the solvent was removed *in vacuo* and the resulting brown solid (8.97 g) was used without further purification or characterization.

Synthesis of CpCp*TaCl₂. The title compound was prepared according to a procedure adapted from the literature.^{26c} While cooling to -84 °C, a solution of PMe₃ (0.24 mL, 2.3 mmol, 0.4 equiv) in toluene (40 mL) was added to a mixture of crude Cp*TaCl₃(PMe₃) (4.00 g, ~6.3 mmol, ~1.0 equiv) and NaCp-1/3 THF (0.76 g, 6.8 mmol, 1.1 equiv) and the mixture was warmed to room temperature and then heated at 100 °C for 18 h. Solvent removal *in vacuo* gave a green-brown solid that was purified by Soxhlet extraction into toluene (20 mL, 24 h). Concentration of the extract gave a brown solid (1.12 g) that was used without further purification.

Synthesis of KCp* (30). The title compound was prepared according to a procedure adapted from the literature.⁴⁵ 1,2,3,4,5-pentamethylcyclopentadiene (6.00 g, 43.5 mmol, 1.2 equiv) was added slowly to a suspension of potassium hydride (1.50 g, 37.5 mmol, 1.0 equiv) in THF (60 mL), and the mixture was stirred for 18 h, during which a white solid formed. This solid was collected by vacuum filtration, washed with THF (30 mL), and dried *in vacuo* to give a fine white solid (4.50 g, 25.8 mmol, 69% yield). Spectral data are consistent with those previously reported.⁴⁵

Synthesis of CpCp*TaH₃ (2). The title compound was prepared according to a procedure adapted from the literature.^{26c} While cooling to -84 °C, Et₂O (65 mL) was added to a mixture of CpCp*TaCl₂ (1.10 g, ~2.40 mmol, ~1.0 equiv) and LiAlH₄ (0.54 g, 14.3 mmol, 6.0 equiv) and the mixture was allowed to slowly warm to room temperature and stirred for 24 h. The mixture was cooled to 0 °C and then degassed. Deionized water (0.72 mL, 40.0 mmol, 17 equiv) was added dropwise. The mixture was allowed to slowly warm to room temperature, after which it was extracted into pentane (2 × 30 mL). The solvent was removed from the combined extracts under vacuum

to give an off-white solid (0.59 g, 65% yield). Spectral data are consistent with those previously reported.^{26c}

Synthesis of Cp*₂TaCl₂. The title compound was prepared according to a procedure adapted from the literature.^{26c} While cooling to -84 °C, a solution of PMe₃ (0.05 mL, 0.50 mmol) in toluene (25 mL) was added to a mixture of crude Cp*TaCl₃(PMe₃) (4.00 g) and KCp* (1.30 g, 7.46 mmol) and the mixture was warmed to room temperature and then heated at 100 °C for 18 h. Solvent removal *in vacuo* gave a brown solid that was purified via Soxhlet extraction into toluene (25 mL, 24 h). Concentration of the extract gave a brown solid (2.27 g) that was used without further purification or characterization.

Synthesis of Cp*₂TaH₃ (3). The title compound was prepared according to a procedure adapted from the literature.^{25a} While cooling to -84 °C, Et₂O (30 mL) was added to a mixture of Cp*₂TaCl₂ (0.50 g, 0.96 mmol, 1.0 equiv) and LiAlH₄ (0.25 g, 6.6 mmol, 6.9 equiv) and the mixture was allowed to slowly warm to room temperature and stirred for 18 h. The mixture was cooled to 0 °C and then degassed. Deionized water (1.0 mL, 55.5 mmol, 57.9 equiv) was added dropwise. The mixture was allowed to slowly warm to room temperature, after which it was extracted into pentane (2 × 25 mL), and the solvent was removed from the combined extracts *in vacuo* to give an off-white solid (0.36 g, 0.79 mmol, 84% yield). Spectral data are consistent with those previously reported.^{26c}

■ COMPUTATIONAL SECTION

Calculations were performed with Gaussian 16.⁴⁶ An ultrafine integration grid and the keyword Sd were used for all calculations. Except when evaluating other methods as specified in the Supporting Information, geometry optimizations of the stationary points were carried out in the gas phase with the M06L¹⁷ functional with BS1 (BS1 = the LANL2DZ pseudopotential for Ta and the 6-31+G(d,p) basis for all other atoms). Frequency analyses were carried out at the same level to evaluate the zero-point vibrational energy and thermal corrections at 298 K. The nature of the stationary points was determined in each case according to the appropriate number of negative eigenvalues of the Hessian matrix. Forward and reverse intrinsic reaction coordinate calculations were carried out on the optimized transition structures to ensure that they indeed connect the appropriate reactants and products.⁴⁷ Multiple conformations and configurations were considered for all structures, and the lowest energy structures are reported. Unless otherwise specified in the Supporting Information, single-point energy calculations were performed with the M06¹⁸ functional with BS2 (BS2 = the SDD pseudopotential for Ta and the 6-311++G(2d,p) basis set for all other atoms). Bulk solvent effects in benzene for computations in Schemes 2 and 5, and toluene for computations in Scheme 4, were considered implicitly in the single-point energy calculations through the CPCM solvation model.⁴⁸ Bond lengths were measured using Gaussview 5.0,⁴⁹ and cyclopentadienyl plane angles were measured using Mercury 3.0.⁵⁰

■ ASSOCIATED CONTENT

Supporting Information

The Supporting Information is available free of charge at <https://pubs.acs.org/doi/10.1021/acs.organomet.1c00308>.

NMR spectra, rate data, computational details, and energies of calculated structures (PDF)

Cartesian coordinates of calculated structures (XYZ)

AUTHOR INFORMATION

Corresponding Author

Sharon R. Neufeldt – Department of Chemistry and Biochemistry, Montana State University, Bozeman, Montana 59717, United States; orcid.org/0000-0001-7995-3995; Email: sharon.neufeldt@montana.edu

Authors

Steven M. Rehbein – Department of Chemistry and Biochemistry, Montana State University, Bozeman, Montana 59717, United States; orcid.org/0000-0002-9240-1260
Matthew J. Kania – Department of Chemistry and Biochemistry, Montana State University, Bozeman, Montana 59717, United States; orcid.org/0000-0003-4445-9780

Complete contact information is available at:
<https://pubs.acs.org/10.1021/acs.organomet.1c00308>

Notes

The authors declare no competing financial interest.

ACKNOWLEDGMENTS

Acknowledgement is made to the donors of The American Chemical Society Petroleum Research Fund (57849-DNI3) and to Montana State University for support of this research. Calculations were performed on Comet at SDSC and Bridges-2 at the Pittsburgh Supercomputing Center through XSEDE (CHE170089), which is supported by NSF (ACI-1548562), and on the Hyalite High-Performance Computing System at MSU. NMR spectra were recorded on an instrument funded by NSF (NSF-MRI:DBI-1532078) and the Murdock Charitable Trust Foundation (2015066:MNL). The authors thank Brian Tripet, Thomas Livinghouse, Michael Mock, and Nicholas Stadie for helpful discussions and the MSU NMR Core Facility for their expertise. Emily K. Reeves is gratefully acknowledged for early work on this project.

REFERENCES

- (1) Kepp, K. P. A quantitative scale of oxophilicity and thiophilicity. *Inorg. Chem.* **2016**, *55*, 9461–9470.
- (2) Beaumier, E. P.; Pearce, A. J.; See, X. Y.; Tonks, I. A. Modern applications of low-valent early transition metals in synthesis and catalysis. *Nat. Rev. Chem.* **2019**, *3*, 15–34.
- (3) (a) Hartwig, J. *Organotransition Metal Chemistry: From Bonding to Catalysis*, 1st ed; University Science Books: Melville, New York, 2010. (b) Crabtree, R. H. *The Organometallic Chemistry of the Transition Metals*, 7th ed; John Wiley & Sons Inc.: Hoboken, New Jersey, 2019.
- (4) Selected reviews: (a) Shilov, A. E.; Shul'pin, G. B. Activation of C–H bonds by metal complexes. *Chem. Rev.* **1997**, *97*, 2879–2932. (b) Labinger, J. A.; Bercaw, J. E. Understanding and exploiting C–H bond activation. *Nature* **2002**, *417*, 507–514. (c) Chirik, P. J. Group 4 Transition Metal Sandwich Complexes: Still Fresh after Almost 60 Years. *Organometallics* **2010**, *29*, 1500–1517. (d) Kuhl, N.; Hopkinson, M. N.; Wencel-Delord, J.; Glorius, F. Beyond Directing Groups: Transition-Metal-Catalyzed C–H Activation of Simple Arenes. *Angew. Chem., Int. Ed.* **2012**, *51*, 10236–10254. (e) Xue, X.-S.; Ji, P.; Zhou, B.; Cheng, J.-P. The Essential Role of Bond Energetics in C–H Activation/Functionalization. *Chem. Rev.* **2017**, *117*, 8622–8648.
- (5) Selected reviews: (a) Fryzuk, M. D.; Johnson, S. A. The continuing story of dinitrogen activation. *Coord. Chem. Rev.* **2000**, *200–202*, 379–409. (b) Ohki, Y.; Fryzuk, M. D. Dinitrogen Activation by Group 4 Metal Complexes. *Angew. Chem., Int. Ed.* **2007**, *46*, 3180–3183. (c) Tanaka, H.; Nishibayashi, Y.; Yoshizawa, K. Interplay between Theory and Experiment for Ammonia Synthesis

Catalyzed by Transition Metal Complexes. *Acc. Chem. Res.* **2016**, *49*, 987–995. (d) Burford, R. J.; Yeo, A.; Fryzuk, M. D. Dinitrogen activation by group 4 and group 5 metal complexes supported by phosphine-amido containing ligand manifolds. *Coord. Chem. Rev.* **2017**, *334*, 84–99.

(6) Representative examples: (a) Mindaola, D. J. Oxidatively Induced Abstraction Reactions. A Synthetic Approach to Low-Coordinate and Reactive Early Transition Metal Complexes Containing Metal–Ligand Multiple Bonds. *Acc. Chem. Res.* **2006**, *39*, 813–821. (b) Nomura, K.; Zhang, S. Design of Vanadium Complex Catalysts for Precise Olefin Polymerization. *Chem. Rev.* **2011**, *111*, 2342–2362. (c) Waterman, R. σ -Bond Metathesis: A 30-Year Retrospective. *Organometallics* **2013**, *32*, 7249–7263.

(7) (a) Bailey, B. C.; Fan, H.; Baum, E. W.; Huffman, J. C.; Baik, M.-H.; Mindaola, D. J. Intermolecular C–H Bond Activation Promoted by a Titanium Alkylidyne. *J. Am. Chem. Soc.* **2005**, *127*, 16016–16017. (b) Flores, J. A.; Cavaliere, V. N.; Buck, D.; Pintér, B.; Chen, G.; Crestani, M. G.; Baik, M.-H.; Mindaola, D. J. Methane activation and exchange by titanium-carbon multiple bonds. *Chem. Sci.* **2011**, *2*, 1457–1462.

(8) Schaller, C. P.; Wolczanski, P. T. Methane vs Benzene Activation via Transient ${}^t\text{Bu}_3\text{SiNHTa}(=\text{NSi}^t\text{Bu}_3)_2$: Structure of $(\text{py})_2\text{MeTa}(=\text{NSi}^t\text{Bu}_3)_2$. *Inorg. Chem.* **1993**, *32*, 131–144.

(9) Examples: (a) Curtis, M. D.; Bell, L. G.; Butler, W. M. C–H Activation. Synthesis of Silyl Derivatives of Niobocene and Tantalocene Hydrides, Their H/D Exchange Reactions with C_6D_6 , and the Structure of $\text{Cp}_2\text{Ta}(\text{H})_2\text{SiMe}_2\text{Ph}$. *Organometallics* **1985**, *4*, 701–707. (b) Jiang, Q.; Pestana, D. C.; Carroll, P. J.; Berry, D. H. Thermochemical Aspects of Arene C–H Activation by Tantalum Silyl Complexes: Relative Ta–Si and Ta–C Bond Enthalpies. *Organometallics* **1994**, *13*, 3679–3691. (c) Li, C.; Dinoi, C.; Coppel, Y.; Etienne, M. CH Bond Activation of Methane by a Transient η^2 -Cyclopropene/Metallabicyclobutane Complex of Niobium. *J. Am. Chem. Soc.* **2015**, *137*, 12450–12453.

(10) Soulivong, D.; Norsic, S.; Taoufik, M.; Copéret, C.; Thivolle-Cazat, J.; Chakka, S.; Basset, J.-M. Non-Oxidative Coupling Reaction of Methane to Ethane and Hydrogen Catalyzed by the Silica-Supported Tantalum Hydride: $(\text{SiO})_2\text{Ta-H}$. *J. Am. Chem. Soc.* **2008**, *130*, 5044–5045.

(11) (a) Vidal, V.; Théolier, A.; Thivolle-Cazat, J.; Basset, J.-M. Metathesis of Alkanes Catalyzed by Silica-Supported Transition Metal Hydrides. *Science* **1997**, *276*, 99–102. (b) Thieuleux, C.; Copéret, C.; Dufaud, V.; Marangeli, C.; Kuntz, E.; Basset, J.-M. Heterogeneous well-defined catalysts for metathesis of inert and not so inert bonds. *J. Mol. Catal. A: Chem.* **2004**, *213*, 47–57. (c) Basset, J. M.; Copéret, C.; Lefort, L.; Maunders, B. M.; Maury, O.; Le Roux, E.; Saggio, G.; Soignier, S.; Soulivong, D.; Sunley, G. J.; Taoufik, M.; Thivolle-Cazat, J. Primary Products and Mechanistic Considerations in Alkane Metathesis. *J. Am. Chem. Soc.* **2005**, *127*, 8604–8605. (d) Le Roux, E.; Taoufik, M.; Copéret, C.; de Mallmann, A.; Thivolle-Cazat, J.; Basset, J.-M.; Maunders, B. M.; Sunley, G. J. Development of Tungsten-Based Heterogeneous Alkane Metathesis Catalysts Through a Structure–Activity Relationship. *Angew. Chem., Int. Ed.* **2005**, *44*, 6755–6758. (e) Chen, Y.; Edy, A.; Ali, H.; Bilel, H.; Lyndon, E.; Basset, J. M. Alkane Metathesis with the Tantalum Methylidene $[(\equiv\text{SiO})\text{Ta}(\text{:CH}_2)\text{Me}_2]/[(\equiv\text{SiO})_2\text{Ta}(\text{:CH}_2)\text{Me}]$ Generated from Well-Defined Surface Organometallic Complex $[(\equiv\text{SiO})\text{Ta}^V\text{Me}_4]$. *J. Am. Chem. Soc.* **2015**, *137*, 588–591.

(12) Pasha, F. A.; Cavallo, L.; Basset, J. M. Mechanism of n-Butane Hydrogenolysis Promoted by Ta-Hydrides Supported on Silica. *ACS Catal.* **2014**, *4*, 1868–1874.

(13) Vidal, V.; Théolier, A.; Thivolle-Cazat, J.; Basset, J.-M. Activation and Functionalisation of the C–H Bonds of Methane and Higher Alkanes by a Silica-supported Tantalum Hydride Complex. *J. Chem. Soc., Chem. Commun.* **1995**, 991–992.

(14) Based on computations, Lin and coworkers favor an alternative pathway involving oxidative addition at low-valent d^2 Ta(III) that stands in contrast to work by Cavallo and Basset (ref 12) Lin, X.; Xi, Y.; Zhang, G.; Phillips, D. L.; Guo, W. A Reaction Mechanism of

Methane Coupling on a Silica-Supported Single-Site Tantalum Catalyst. *Organometallics* **2014**, *33*, 2172–2181.

(15) Selected examples: (a) Buckner, S. W.; MacMahon, T. J.; Byrd, G. D.; Freiser, B. S. Gas-phase reactions of niobium(1+) and tantalum(1+) with alkanes and alkenes. Carbon-hydrogen bond activation and ligand-coupling mechanisms. *Inorg. Chem.* **1989**, *28*, 3511–3518. (b) Wesendrup, R.; Schwarz, H. Tantalum-Mediated Coupling of Methane and Carbon Dioxide in the Gas Phase. *Angew. Chem., Int. Ed.* **1995**, *34*, 2033–2035. (c) Parke, L. G.; Hinton, C. S.; Armentrout, P. B. Experimental and Theoretical Studies of the Activation of Methane by Ta+. *J. Phys. Chem. C* **2007**, *111*, 17773–17787. (d) Lapoutre, V. J. F.; Redlich, B.; van der Meer, A. F. G.; Oomens, J.; Bakker, J. M.; Sweeney, A.; Mookherjee, A.; Armentrout, P. B. Structures of the Dehydrogenation Products of Methane Activation by 5d Transition Metal Cations. *J. Phys. Chem. A* **2013**, *117*, 4115–4126. (e) Eckhard, J. F.; Masubuchi, T.; Tschurl, M.; Barnett, R. N.; Landman, U.; Heiz, U. Thermal Dehydrogenation of Methane Enhanced by μ^2 -Oxo Ligands in Tantalum Cluster Cations [TaxO]⁺, x = 4, 5. *J. Phys. Chem. C* **2018**, *122*, 25628–25637.

(16) (a) Barefield, E. K.; Parshall, G. W.; Tebbe, F. N. Catalysis of Aromatic Hydrogen-Deuterium Exchange by Metal Hydrides. *J. Am. Chem. Soc.* **1970**, *92*, 5234–5235. (b) Parshall, G. W. Intramolecular aromatic substitution in transition metal complexes. *Acc. Chem. Res.* **1970**, *3*, 139–144. (c) Parshall, G. W.; Tebbe, F. N. Hydride Derivatives of Niobocene and Tantalocene. *J. Am. Chem. Soc.* **1971**, *93*, 3793–3795. (d) Klabunde, U.; Parshall, G. W. Activation of Aromatic Carbon-Hydrogen Bonds by Transition Metal Complexes. II. Substituted Benzenes. *J. Am. Chem. Soc.* **1972**, *94*, 9081–9087. (e) Foust, D. F.; Rogers, R. D.; Rausch, M. D.; Atwood, J. L. Photoinduced Reactions of $(\eta^5\text{-C}_5\text{H}_5)_2\text{M}(\text{CO})\text{H}$ (M = Nb, Ta) and the Molecular Structure of $(\eta^5\text{-C}_5\text{H}_5)_2\text{Ta}(\text{CO})\text{H}$. *J. Am. Chem. Soc.* **1982**, *104*, 5646–5650.

(17) Zhao, Y.; Truhlar, D. G. A New Local Density Functional for Main-Group Thermochemistry, Transition Metal Bonding, Thermochemical Kinetics, and Noncovalent Interactions. *J. Chem. Phys.* **2006**, *125*, 194101.

(18) Zhao, Y.; Truhlar, D. G. The M06 suite of density functionals for main group thermochemistry, thermochemical kinetics, non-covalent interactions, excited states, and transition elements: two new functionals and systematic testing of four M06-class functionals and 12 other functionals. *Theor. Chem. Acc.* **2008**, *120*, 215–241.

(19) Moltved, K. A.; Kepp, K. P. Chemical Bond Energies of 3d Transition Metals Studied by Density Functional Theory. *J. Chem. Theory Comput.* **2018**, *14*, 3479–3492.

(20) (a) Brookes, N. J.; Ariafard, A.; Stranger, R.; Yates, B. F. Scission of Carbon Monoxide Using TaR₃, R = (N(tBu)Ph) or OSi(tBu)₃: A DFT Investigation. *Chem.—Eur. J.* **2010**, *16*, 8117–8132. (b) Solans-Monfort, X.; Chow, C.; Gouré, E.; Kaya, Y.; Basset, J.-M.; Taoufik, M.; Quadrelli, E. A.; Eisenstein, O. Successive Heterolytic Cleavages of H₂ Achieve N₂ Splitting on Silica-Supported Tantalum Hydrides: A DFT Proposed Mechanism. *Inorg. Chem.* **2012**, *51*, 7237–7249. (c) Núñez-Zarur, F.; Solans-Monfort, X.; Restrepo, A. Mechanistic Insights into Alkane Metathesis Catalyzed by Silica-Supported Tantalum Hydrides: A DFT Study. *Inorg. Chem.* **2017**, *56*, 10458–10473.

(21) (a) Cramer, C. J.; Truhlar, D. G. Density functional theory for transition metals and transition metal chemistry. *Phys. Chem. Chem. Phys.* **2009**, *11*, 10757–10816. (b) Neese, F. A critical evaluation of DFT, including time-dependent DFT, applied to bioinorganic chemistry. *J. Biol. Inorg. Chem.* **2006**, *11*, 702–711.

(22) Reductive elimination of H₂ from silica-supported tantalum hydrides has also been found to be barrierless based on DFT calculations; see ref 12.

(23) Woo, T. K.; Blöchl, P. E.; Ziegler, T. Monomer Capture in Brookhart's Ni(II) Diimine Olefin Polymerization Catalyst: Static and Dynamic Quantum Mechanics/Molecular Mechanics Study. *J. Phys. Chem. A* **2000**, *104*, 121–129.

(24) H–H activation via a σ -bond metathesis pathway was ruled out on the basis of parahydrogen induced polarization experiments:

(a) Millar, S. P.; Zubris, D. L.; Bercaw, J. E.; Eisenberg, R. On the Mechanism of Dihydrogen Addition to Tantalocene Complexes. *J. Am. Chem. Soc.* **1998**, *120*, 5329–5330. (b) Bregel, D. C.; Oldham, S. M.; Eisenberg, R. Mechanistic Studies on the Addition of Dihydrogen to Tantalocene Complexes. *J. Am. Chem. Soc.* **2002**, *124*, 13827–13832.

(25) (a) Findlay, A. E.; Leelasubcharoen, S.; Kuzmina, L. G.; Howard, J. A. K.; Nikonov, G. I. Phosphido-bridged Ta/Rh bimetallic complex: synthesis, structure, and catalytic hydrosilylation of acetophenone. *Dalton Trans.* **2010**, *39*, 9264–9269. (b) Schmidt, S.; Sundermeyer, J. Höherwertige Derivate der d-Metall-Säuren X. Imidokomplexe des fünf- und vierwertigen Niob und Tantal mit Halbsandwich- und Metallocen-Struktur. *J. Organomet. Chem.* **1994**, *472*, 127–138. (c) Korolev, A. V.; Rheingold, A. L.; Williams, D. S. A General Route to Labile Niobium and Tantalum d⁰ Monoimides. Discussion of Metal-Nitrogen Vibrational Modes. *Inorg. Chem.* **1997**, *36*, 2647–2655.

(26) Various highly colored group 5 M(III)-aluminate species intermediate in the preparation of the M(V) metallocene trihydrides are known, from red (a) to orange (b) to yellow (c). However, we have observed none of the characteristic high-upfield ¹H NMR signals corresponding to the bridging hydrides in these and similar aluminates in our samples: (a) Fryzuk, M. D.; Clentsmith, G. K. B.; Rettig, S. J. Coordination behavior of LiBEt₄ towards $(\eta^5\text{-C}_5\text{H}_5)_2\text{ReH}$, $(\eta^5\text{-C}_5\text{H}_5)_2\text{WH}_2$ and $(\eta^5\text{-C}_5\text{H}_5)_2\text{TaH}_3$. Solid state structure of $[(\eta^5\text{-C}_5\text{H}_5)_2\text{TaH} \cdot \text{AlH}_2(\text{OCH}_2\text{CH}_2\text{CH}_2\text{CH}_3)]_2$. *Inorg. Chim. Acta* **1997**, *259*, 51–59. (b) Labinger, J. A.; Wong, K. S. Mechanism of Formation of $(\eta^5\text{-C}_5\text{H}_5)_2\text{NbH}_3$ from the Reaction of $(\eta^5\text{-C}_5\text{H}_5)_2\text{NbCl}_2$ with Hydroaluminate Reducing Agents. *J. Organomet. Chem.* **1979**, *170*, 373–384. (c) Gibson, V. C.; Bercaw, J. E.; Bruton, W. J.; Sanner, R. D. “Bent-Sandwich” Derivatives of Tantalum Bearing One or Two Pentamethylcyclopentadienyl Ligands. *Organometallics* **1986**, *5*, 976–979.

(27) Elevated pressures were utilized in these experiments to increase the solvent boiling point above the temperature of the heating block in order to avoid ambiguity about the actual reaction temperature.

(28) The absorbance maximum of Cp₂TaH₃ is at 235 nm (see Supporting Information). However, irradiation of Cp₂TaH₃ at 254 nm (the closest available wavelength match for our Rayonet photochemical reactor) results in rapid catalyst decomposition. We have found the use of 350 nm lamps to be the best compromise between promoting catalysis while limiting decomposition. This result is in agreement with previous observations Margulieux, G. W.; Semproni, S. P.; Chirik, P. J. Photochemically Induced Reductive Elimination as a Route to a Zirconocene Complex with a Strongly Activated N₂ Ligand. *Angew. Chem., Int. Ed.* **2014**, *53*, 9189–9192.

(29) An additional potentially complicating factor with irradiating near the absorbance maximum of Cp₂TaH₃ is the isomerization of benzene to fulvene and benzvalene that could complicate analysis and likely provide species that are more reactive than benzene itself. For examples, see: (a) Wilzbach, K. E.; Ritscher, J. S.; Kaplan, L. Benzvalene, the tricyclic valence isomer of benzene. *J. Am. Chem. Soc.* **1967**, *89*, 1031–1032. (b) Kaplan, L.; Wilzbach, K. E. Photolysis of benzene vapor. Benzvalene formation at wavelengths 2537–2370 Å. *J. Am. Chem. Soc.* **1968**, *90*, 3291–3292.

(30) Though the exact species responsible for the red coloration of these samples remains elusive, a strong candidate is that of the paramagnetic (¹H NMR silent) 17e⁻ species $(\eta^5\text{-C}_5\text{H}_5)_2\text{TaH}_2$, resulting from photochemically-induced radical abstraction of a single hydrogen from I. For literature support, see (a) which includes EPR spectroscopy (but not isolation) of $(\eta^5\text{-C}_5\text{H}_5)_2\text{TaH}_2$ and EPR spectroscopy and isolation of the deep-red isoelectronic paramagnetic complex $(\eta^5\text{-CH}_3\text{C}_5\text{H}_5)_2\text{Ta}(\text{CH}_3)_2$ and (b) which includes isolation of a photochemically generated 17e⁻ species in a low-temperature matrix: (a) Elson, I. H.; Kochi, J. K.; Klabunde, U.; Manzer, L. E.; Parshall, G. W.; Tebbe, F. N. Paramagnetic hydride and alkyl complexes of niobium(IV) and tantalum(IV). *J. Am. Chem. Soc.* **1974**, *96*, 7374–7376. (b) Baynham, R. F. G.; Chetwynd-Talbot, J.;

Grebenik, P.; Perutz, R. N.; Powell, M. H. A. Photochemistry of $M(\eta^5\text{-C}_5\text{H}_5)_2(\text{H})\text{CO}$ and $M(\eta^5\text{-C}_5\text{H}_5)_2\text{H}_3$ ($M = \text{Nb, Ta}$) in low temperature matrices. *J. Organomet. Chem.* **1985**, *284*, 229–242.

(31) Deutsch, P. P.; Maguire, J. A.; Jones, W. D.; Eisenberg, R. Hydride abstraction. The reaction of [bis(diphenylphosphino)ethane]carbonylhaloiridium with bis(cyclopentadienyl)-trihydridotantalum. *Inorg. Chem.* **1990**, *29*, 686–690.

(32) (a) Jia, C.; Kitamura, T.; Fujiwara, Y. Catalytic Functionalization of Arenes and Alkanes via C–H Bond Activation. *Acc. Chem. Res.* **2001**, *34*, 633–639. (b) Walton, J. W.; Wilkinson, L. A.; Paymore, N. J.; Elliot, P. P. π -Coordinated arene metal complexes and catalysis. *Organometallic Chemistry: Volume 42*; Royal Society of Chemistry: Cambridge, U.K., 2019; pp 125–171. (c) Rej, S.; Das, A.; Chatani, N. Strategic evolution in transition metal-catalyzed directed C–H bond activation and future directions. *Coord. Chem. Rev.* **2021**, *431*, 213683. (d) Williams, L. J.; Bhonoah, Y.; Wilkinson, L. A.; Walton, J. W. As Nice as π : Aromatic Reactions Activated by π -Coordination to Transition Metals. *Chem.—Eur. J.* **2021**, *27*, 3650–3660.

(33) For a closely related insertion into a C–F bond, see Gianetti, T. L.; Bergman, R. G.; Arnold, J. Carbon–fluorine bond cleavage in fluoroarenes via a niobium(III) imido complex: from stoichiometric to catalytic hydrodefluorination. *Chem. Sci.* **2014**, *5*, 2517–2524.

(34) (a) Brintzinger, H.; Bercaw, J. E. Bis(pentamethylcyclopentadienyl)titanium(II). Isolation and Reactions with Hydrogen, Nitrogen, and Carbon Monoxide. *J. Am. Chem. Soc.* **1971**, *93*, 2045–2046. (b) McLain, S. J.; Wood, C. D.; Schrock, R. R. Preparation and Characterization of Tantalum(III) Olefin Complexes and Tantalum(V) Metallacyclopentane Complexes Made from Acyclic α Olefins. *J. Am. Chem. Soc.* **1979**, *101*, 4558–4570. (c) McLain, S. J.; Sancho, J.; Schrock, R. R. Metallacyclopentane to Metallacyclobutane Ring Contraction. *J. Am. Chem. Soc.* **1979**, *101*, 5451–5453. (d) McLain, S. J.; Sancho, J.; Schrock, R. R. Selective Dimerization of Monosubstituted α -Olefins by Tantalacyclopentane Catalysts. *J. Am. Chem. Soc.* **1980**, *102*, 5610–5618. (e) Van Asselt, A.; Burger, B. J.; Gibson, V. C.; Bercaw, J. E. Hydrido methylidene, hydrido vinylidene, hydrido oxo, and hydrido formaldehyde derivatives of bis(pentamethylcyclopentadienyl)tantalum. *J. Am. Chem. Soc.* **1986**, *108*, 5347–5349. (f) Antonelli, D. M.; Schaefer, W. P.; Parkin, G.; Bercaw, J. E. Synthesis and characterization of $(\eta^5\text{-C}_5\text{Me}_5)_2\text{TaCl}$ (THF), a useful synthetic precursor for the preparation of oxo, imido and methylidene derivatives of permethyltantalocene. *J. Organomet. Chem.* **1993**, *462*, 213–220.

(35) The downfield trend of the hydride signals with increasing methylation of the Cp rings is perhaps counterintuitive, since the permethylated ligands are more electron-rich than the unmethylated Cp rings. However, this trend is consistent with a slight elongation of the Ta–ligand distance with permethylation. With increasing methylation, the average distance between Ta and the centroid of the Cp (or Cp*) ligands increases, presumably due to sterics, suggesting less electron donation from Cp (Cp*) to tantalum (see Table 2, complexes 1, 8, and 9).

(36) Gibson, V. C.; Parkin, G.; Bercaw, J. E. Synthesis and reactivity of permethyltantalocene derivatives processing η^3 -allyl, η^2 -butadiene, η^2 -methylallene, and η^1 -alkenylidene ligands. Model studies for the role of surface vinylidenes in the Fischer-Tropsch hydrocarbon-chain-lengthening process. *Organometallics* **1991**, *10*, 220–231.

(37) Although we have not observed H/D exchange between $\text{Cp}_2^*\text{TaH}_3$ and C_6D_6 under N_2 , a modest amount of H/D exchange between $\text{Cp}_2^*\text{TaH}_3$ and D_2 can be observed at extended reaction times.

(38) Green, J. C. Bent metallocenes revisited. *Chem. Soc. Rev.* **1998**, *27*, 263–271.

(39) Wolfsberger, W.; Schmidbauer, H. Eine befreundende darstellungsmethode für trimethylphosphin. *Synth. React. Inorg. Met.-Org. Chem.* **1974**, *4*, 149–156.

(40) Performing evacuation-refill cycles with N_2 (analogous to those performed with H_2 or D_2) was found to not affect reaction rate. As

such, the rate depression observed in experiments under pressures of H_2 or D_2 is not related to the multiple evacuation-refill cycles.

(41) Tay, B.-Y.; Wang, C.; Stubbs, L. P.; Jacob, C.; van Meurs, M. Deuterated dimethyl sulfoxide as a good NMR solvent for the characterization of alkali metal cyclopentadienides, amides, alkoxides and phenoxides. *J. Organomet. Chem.* **2011**, *696*, 3431–3435.

(42) This and all other -84°C cold baths were prepared from ethyl acetate and liquid nitrogen.

(43) Thomson, R. K.; Monreal, M. J.; Masuda, J. D.; Scott, B. L.; Kiplinger, J. L. Lutetium gets a crown: Synthesis, structure and reaction chemistry of the separated ion pair complex, $[\text{Li}(12\text{-crown-4})_2][(\text{C}_5\text{Me}_5)_2\text{LuMe}_2]$. *J. Organomet. Chem.* **2011**, *696*, 3966–3973.

(44) Sanner, R. D.; Carter, S. T.; Bruton, W. J., Jr. The preparation of mono(η^5 -pentamethylcyclopentadienyl) compounds of tantalum(V). *J. Organomet. Chem.* **1982**, *240*, 157–162.

(45) Rabe, G.; Roesky, H. W.; Stalke, D.; Pauer, F.; Sheldrick, G. M. The preparation and crystal structures of sodium and potassium pentamethylcyclopentadienyl pyridine solvates. *J. Organomet. Chem.* **1991**, *403*, 11–19.

(46) Frisch, M. J.; Trucks, G. W.; Schlegel, H. B.; Scuseria, G. E.; Robb, M. A.; Cheeseman, J. R.; Scalmani, G.; Barone, V.; Petersson, G. A.; Nakatsuji, H.; Li, X.; Caricato, M.; Marenich, A. V.; Bloino, J.; Janesko, B. G.; Gomperts, R.; Mennucci, B.; Hratchian, H. P.; Ortiz, J. V.; Izmaylov, A. F.; Sonnenberg, J. L.; Williams-Young, D.; Ding, F.; Lipparini, F.; Egidi, F.; Goings, J.; Peng, B.; Petrone, A.; Henderson, T.; Ranasinghe, D.; Zakrzewski, V. G.; Gao, J.; Rega, N.; Zheng, G.; Liang, W.; Hada, M.; Ehara, M.; Toyota, K.; Fukuda, R.; Hasegawa, J.; Ishida, M.; Nakajima, T.; Honda, Y.; Kitao, O.; Nakai, H.; Vreven, T.; Throssell, K.; Montgomery, J. A., Jr.; Peralta, J. E.; Ogliaro, F.; Bearpark, M. J.; Heyd, J. J.; Brothers, E. N.; Kudin, K. N.; Staroverov, V. N.; Keith, T. A.; Kobayashi, R.; Normand, J.; Raghavachari, K.; Rendell, A. P.; Burant, J. C.; Iyengar, S. S.; Tomasi, J.; Cossi, M.; Millam, J. M.; Klene, M.; Adamo, C.; Cammi, R.; Ochterski, J. W.; Martin, R. L.; Morokuma, K.; Farkas, O.; Foresman, J. B.; Fox, D. J. *Gaussian 16*; Gaussian Inc.: Wallingford CT, 2016.

(47) (a) Gonzalez, C.; Schlegel, H. B. An Improved Algorithm for Reaction Path Following. *J. Chem. Phys.* **1989**, *90*, 2154–2161.

(b) Gonzalez, C.; Schlegel, H. B. Reaction Path Following in Mass-Weighted Internal Coordinates. *J. Phys. Chem.* **1990**, *94*, 5523–5527.

(c) Fukui, K. The Path of Chemical Reactions - the IRC Approach. *Acc. Chem. Res.* **1981**, *14*, 363–368.

(48) Cossi, M.; Rega, N.; Scalmani, G.; Barone, V. Energies, structures, and electronic properties of molecules in solution with the C-PCM solvation model. *J. Comput. Chem.* **2003**, *24*, 669–681.

(49) Dennington, R.; Keith, T. A.; Millam, J. M. *GaussView*, Version 6; Semichem Inc.: Shawnee Mission, KS, 2016.

(50) Macrae, C. F.; Bruno, I. J.; Chisholm, J. A.; Edgington, P. R.; McCabe, P.; Pidcock, E.; Rodriguez-Monge, L.; Taylor, R.; van de Streek, J.; Wood, P. A. Mercury CSD 2.0 - new features for the visualization and investigation of crystal structures. *J. Appl. Crystallogr.* **2008**, *41*, 466–470.